Quadcopter Noise Predictions with Wall-Modeled Large Eddy Simulations

Man-Long WONG, Gaetan K. W. KENWAY, Aditya S. GHATE, Jordan B. ANGEL, and Cetin C. KIRIS

[1]Volcano Platforms Inc., Palo Alto, CA 94306 USA

Keywords: advanced air mobility (AAM), urban air mobility (UAM), computational aero-acoustics (CAA), computational fluid dynamics (CFD), large eddy simulation (LES), graphics processing unit (GPU)

Abstract Urban air mobility (UAM) introduces unconventional aerial vehicles, such as quadrotors, that pose significant challenges for noise analysis using traditional computational tools. This study demonstrates aero-acoustic predictions of the Straight Up Imaging (SUI) quadcopter using wall-modeled large eddy simulations (WMLES) computed with Volcano ScaLES, a state-of-the-art computational fluid dynamics (CFD) solver, on consumer-grade graphics processing unit (GPU) devices. The WMLES utilize low-dissipative schemes on Cartesian grids with a robust immersed boundary method for imposing effects from complex geometries. Far-field acoustic pressure signals are computed on-the-fly during the simulations with an integrated permeable Ffowcs Williams-Hawkings (FWH) solver. Validation against NASA Langley wind tunnel data shows excellent agreement in rotor blade-passing tones and broadband noise characteristics, demonstrating solver accuracy in noise predictions for UAM applications with short turnaround time and low computational resources.

Introduction

Urban air mobility (UAM), which involves smaller and highly automatic aerial vehicles for urban passenger and cargo transportation at low altitudes, is expected to grow rapidly in coming years due to large economic benefits offered by the faster transportation and alleviation of urban congestion. However, in contrast to traditional aerial vehicles in urban areas, such as helicopters, UAM introduces unconventional types of aerial vehicles, such as the "quadrotor" configuration, for better aerodynamic benefits. Traditional computational fluid dynamics-computational aero-acoustics (CFD-CAA) approaches, such as unsteady Reynolds-averaged Navier—Stokes (RANS), may not be suitable as tools for designing quiet UAM to reduce public disturbance and meet regulatory standards. In this work, we demonstrate the use of the wall-modeled large eddy simulation (WMLES) approach with a CFD framework, Volcano ScaLES, for cost efficient and accurate acoustic prediction in the Straight Up Imaging (SUI) Endurance quadcopter benchmark case. ScaLES is a graphical processing unit (GPU) solver, developed mainly for day-to-day robust CFD large eddy simulations (LES) and is highly suited for analysis of aerodynamics and aero-acoustics during the design stages of different kinds of aerospace vehicles, including the UAM vehicles. The SUI quadcopter model consists of an airframe and four rotors of blades with radii of 190.5 mm, where the distance between rotors is approximately 510 mm. The noise radiated from the SUI quadcopter under different flight conditions was studied experimentally with a linear array of 28 microphones in the flyover configuration in the NASA Langley Low Speed Aeroacoustic Wind Tunnel (LSAWT) of NASA by Pettingill and Zawodny [1, 2]. In this paper, we consider the forward flight case with the angle of attack $\alpha = -10°$ at a freestream Mach number $M_\infty = 0.045$ (freestream velocity magnitude $U_\infty = 15.5$ m/s). The rotor RPMs, geometry of the SUI quadrotor, and the position of the microphones are shown in Fig. 1.

Simulation details

All simulations in this work are conducted with the compressible Navier–Stokes formulation using a nominally fourth-order accurate finite-difference spatial discretization on convective flux with favorable kinetic energy and entropy consistency properties in turbulent regions, and the viscous flux discretization utilizes a mix of fourth and second order discretizations with improved resolution for high Reynolds number turbulent flows. The simulations presented in this work use the Smagorinsky model with dynamic procedure to model the subgrid-scale stress tensor [6, 7]. With the third-order strong stability preserving (SSP) Runge–Kutta (RK) time stepping method, the overall numerical formulation has low dissipation and high isotropy, making it suitable for LES over a vast range of flow regimes with turbulence and acoustic wave radiation. To handle complex geometries at high Reynolds numbers, algebraic wall model is used at walls with a robust immersed boundary method. Far-field acoustics can be computed on-the-fly (in-situ) during the simulations with sampled data on Ffowcs Williams-Hawkings (FWH) surface with a permeable FWH solver [3, 4] incorporated with the CFD solver, where the details can be found in our previous work [8]. ScaLES has recently been validated on a wide variety of CFD applications, such as jet aero-acoustics [8], vibro-acoustics of a space vehicle [9], and many aerodynamic benchmark problems [10, 11, 12]. A unique aspect of the GPU solver, compared to other CFD codes, is that most of the work is compute-bound, so that high performance is achieved even on graphics-oriented, bandwidth-restricted devices, such as RTX 4090 and L40S GPU cards, which are far less expensive than higher memory bandwidth hardware, and make WMLES practical for use in an industrial setting. Rotating geometries are also supported with the sliding mesh capability. In our setup of the quadrotor simulations, four rotating blades are enabled with the corresponding cylindrical sliding meshes. The sliding mesh regions and the permeable FWH surface with 5 end-caps are shown in Fig. 1 (distance between end-caps is 0.1 m). The FWH surface is carefully designed to prevent turbulent wake passing through the surface, except at the end-caps, where the end-cap averaging technique is used to reduce spurious low-frequency noise. Three different grids are designed for the simulations, which are labeled as "coarse", "medium", and "fine" with increasing finest grid spacing, and the grid sizes range from 255.8 million to 2.663 billion cells. Only the grid hierarchy of the medium grid is shown in Fig. 2, but grid hierarchies are essentially the same for the coarse and fine grids. From the figure, it can be seen that finest grid cells are deployed near the geometry of the vehicle and the sliding mesh regions. A large volume refinement region enclosing the FWH sampling surface is also designed for capturing acoustic radiation from the quadrotor to the FWH surface. For the medium grid, this region has a grid resolution of 1.6 mm. We have run all simulations until the 50th revolution of the 1st rotor (at 4047 RPM) and all results in this paper are only based on data sampled after 10th revolution when transient is flushed out. The details of the simulations are given in Table 1. In the experiment, thrust was measured to be 44.6 N. Our simulations predict thrust values with small grid sensitivity in the range of 40.88 to 41.90 N, where all of them have less than 10% error. Note that the experimental error margins on such geometries tend to be large as noted in the single rotor aerodynamic analysis by Russell et al. [5]. As such these simulations are deemed sufficiently accurate to pursue aerodynamic analysis. Note that numerical analysis requiring about 50 revolutions of 1st forward rotor can be completed within one full day for the coarsest grid. Fig. 3 shows the iso-surfaces of Q-criterion from the fine grid, where the vortices generated by the rotors and the complex blade-vortex interaction can be clearly visualized, by using the in-situ ray-tracing visualization implemented in ScaLES.

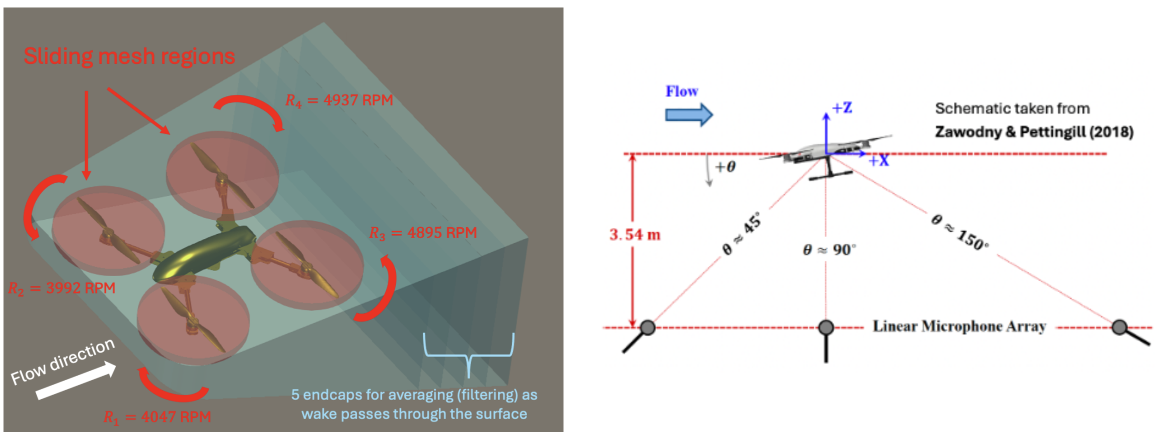

(a) Simulation setup

(b) Experiment microphone setup [2]

Figure 1: *Set-up of sliding mesh regions and FWH surface around SUI quadrotor geometry in the simulations and far-field microphone locations in the experiment [2].*

Table 1: Grid characteristics and computational resources.

Cases	Coarse	Medium	Fine
Minimum grid spacing [mm] (% of tip chord)	0.6 (4.8)	0.4 (3.23)	0.267 (2.15)
Number of cells [million]	255.8	821.7	2663
Explicit time step size [μs]	0.97	0.63	0.43
Wall-clock time per revolution of 1st rotor [hours] (# GPUs used)	0.42 (4x L40S)	0.79 (8x L40S)	1.93 (8x RTX Pro 6000)
Thrust [N]	41.29	40.88	41.90

Results

During the simulations, the acoustic pressure signals at the far-field observers are computed

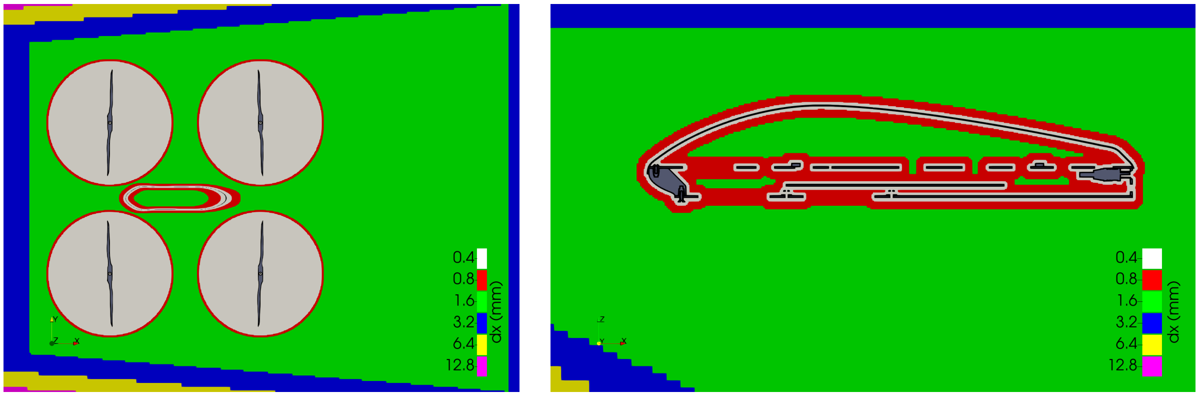

(a) xy-plane ($z = 0.17803$ m) (b) xz-plane ($y = 0$)

Figure 2: *Cross-sections of medium grid showing the grid topology with the grid spacings. The black contour lines show the location of the quadrotor geometry.*

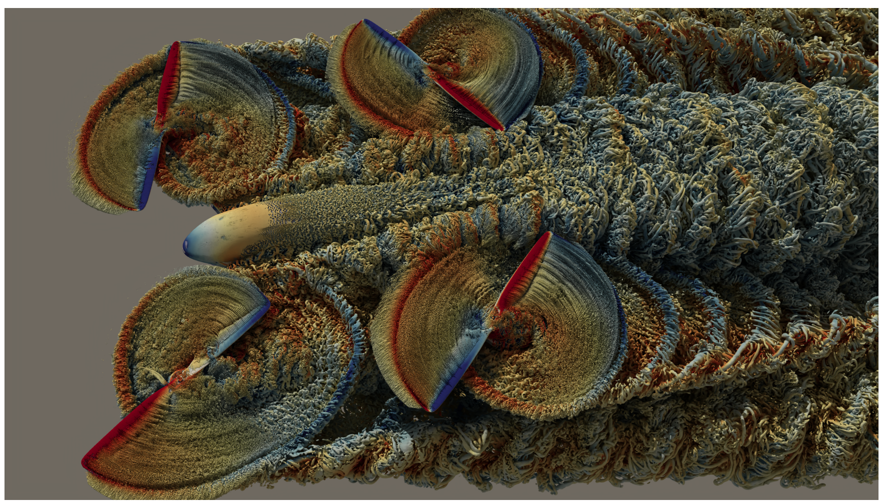

Figure 3: *Iso-surfaces of Q-criterion, colored by the streamwise velocity component, showing the turbulent structures around the quadrotor on the fine grid looking from the top.*

using data sampled at a frequency of 67.45 kHz on the FWH surface triangulation with edge length of approximately 5 mm. We follow the procedures in the experimental work [2] to reproduce the narrow-band spectra. To obtain the spectra, the Welch's method is first employed to compute the power spectral density (PSD) spectra using truncated signal segments at a frequency resolution of 5 Hz. To avoid spectral leakage, the Hann windowing with 90% overlap is used for truncating the full pressure time signals into the segments. Due to the low frequency resolution requirement to capture the low-frequency tones that are as low as around 130 Hz, a long sampling time period is required to obtain spectra that are statistically well-converged in the high-frequency range, even when a 90% overlap is used for the segments. Fig. 4(a) shows the comparison between the simulation and experimental results, using data sampled from 10th to 50th revolution. One can also consider the composite spectra, where different configurations of the Welch's method are used in different frequency ranges of the spectra. The composite spectra from the simulations, with three frequency ranges, 0 to 500 Hz, 500 to 2000 Hz, and 2000 Hz up to the Nyquist frequency, using data from 10th to 35th revolutions are shown in Fig. 4(b). The frequency resolutions are 1 Hz, 5 Hz, and 20 Hz, respectively, for the low-, medium-, and high-frequency ranges and 70% overlap is chosen for all ranges. We can see from the figure that the composite spectra are more statistically converged compared to the regular spectra, especially in the high-frequency range, by using a smaller amount of data. For example, the medium grid simulation can be finished with around one day when composite spectra is considered, while the turn-around time is around 40 hours when the narrow-band spectra is computed in the traditional way.

From both figures, very good predictions are seen for the first two tones associated with the front and rear rotor blade passing frequencies (BPF), especially for the composite spectra, due to lower frequency resolution employed for the low-frequency tones. The predicted peaks of the two lowest tones are also well grid converged even for the coarsest grid. In the very high-frequency range (above 10 kHz), the spectra from the coarsest grid show some inconsistency with those with higher grid resolutions, which is due to the insufficient resolution in resolving the high-frequency acoustic propagation from the quadrotor to the FWH surface. In general, the broadband noise is captured well by simulations. Small discrepancies at very high frequencies between simulation and experimental results may be attributed to some possible aliasing in the experimental data, as the latter shows an unexpected rise above 10 kHz. Overall, the spectra from the medium grid is well grid-converged in the full frequency range of interest (from lowest BPF to 10 kHz).

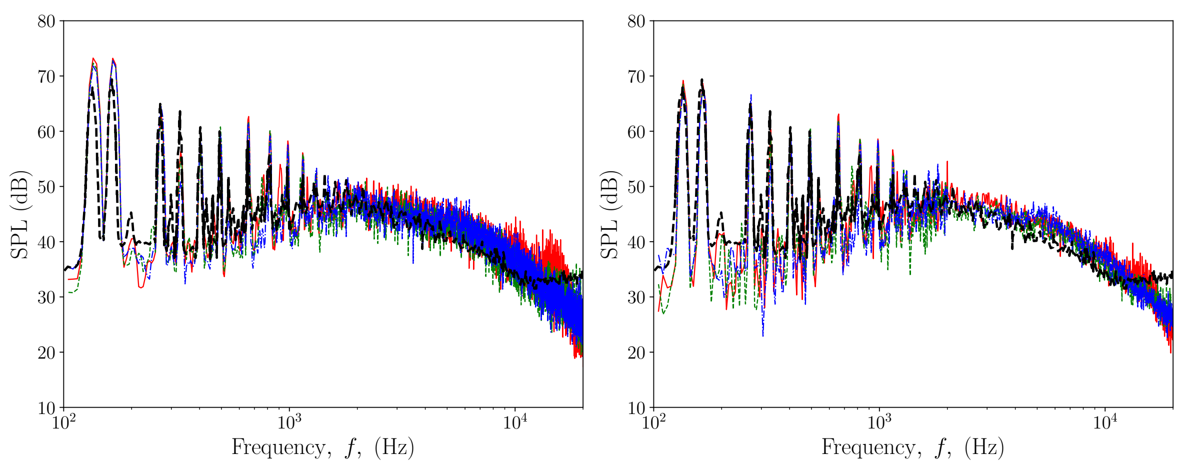

(a) Regular spectra

(b) Composite spectra

Figure 4: *Comparison of narrow-band spectra (sound pressure level, SPL) between simulations and experiment at a chosen microphone ($\theta = 70°$). Red solid line: coarse; green dashed line: medium; blue dash-dotted line: fine; thick black dashed line: experiment.*

Summary

WMLES using the GPU-accelerated Volcano ScaLES solver efficiently predict the aeroacoustic characteristics of the SUI quadcopter in forward flight. The immersed boundary approach and permeable FWH formulation enable accurate noise computation with complex rotor–airframe interactions. Simulation results show excellent agreement with experimental measurements for both tonal and broadband components. Grid-convergence tests confirm that accurate spectra can be obtained on medium grid within short turnaround times, demonstrating the practicality of GPU-based CFD–CAA methods for UAM noise prediction.

Acknowledgments

This work is partially supported by NASA Small Business Innovation Research (SBIR) Phase-I program with contract number: 80NSSC24PB479. We greatly appreciate Carl Russell of NASA Ames Research Center for providing the SUI geometry.

References

[1] N. A. Pettingill, N. S Zawodny, Identification and prediction of broadband noise for a small quadcopter, Vertical Flight Society 75th Annual Forum & Technology Display (2019). https://doi.org/10.4050/F-0075-2019-14443

[2] N. Zawodny, N. Pettingill, Acoustic wind tunnel measurements of a quadcopter in hover and forward flight conditions, INTER-NOISE and NOISE-CON Congress and Conference Proceedings (2018) pp. 487-500.

[3] P. Di Francescantonio, A new boundary integral formulation for the prediction of sound radiation, Journal of Sound and Vibration (1997), pp. 491-509. https://doi.org/10.1006/jsvi.1996.0843

[4] K. S. Brentner, F. Farassat, Analytical comparison of the acoustic analogy and Kirchhoff formulation for moving surfaces, AIAA journal (1998). https://doi.org/10.2514/2.558

[5] C. R. Russell, J. Jung, G. Willink, B. Glasner, Wind tunnel and hover performance test results for multicopter UAS vehicles, Vertical Flight Society 72nd Annual Forum (2016). https://doi.org/10.4050/f-0072-2016-11580

[6] D. K. Lilly, A proposed modification of the Germano subgrid-scale closure method, Physics of Fluids A (1992). https://doi.org/10.1063/1.858280

[7] P. Moin, K. Squires, W. Cabot, S. Lee, A dynamic subgrid-scale model for compressible turbulence and scalar transport, Physics of Fluids A (1991). https://doi.org/10.1063/1.858164

[8] M. L. Wong, A. Ghate, G. K. Kenway, J. B. Angel, C. C. Kiris, Immersed boundary wall-modelled large eddy simulations of subsonic jet flows and acoustics, AIAA Aviation Forum (2024). https://doi.org/10.2514/6.2024-4466

[9] G. K. Kenway, A. Ghate, O. M. Browne, M. L. Wong, J. B. Angel, C. C. Kiris, Immersed boundary wall-modelled large eddy simulations of a generic hammerhead payload fairing, AIAA Aviation Forum (2024). https://doi.org/10.2514/6.2024-3693

[10] N. Ashton, A. Ghate, G. Kenway, J. Angel, M. L. Wong, C. C. Kiris, Immersed boundary wall-modeled large eddy simulations for the 5th High-Lift Prediction Workshop, AIAA SciTech Forum (2025). https://doi.org/10.2514/6.2025-0888

[11] M. L. Wong, A. Ghate, G. K. Kenway, J. B. Angel, C. C. Kiris, Immersed boundary wall-modelled large eddy simulations of straight wings with three-dimensional ice accretion, AIAA Aviation Forum (2024). https://doi.org/10.2514/6.2024-4000

[12] J. B. Angel, M. L. Wong, G. K. Kenway, A. Ghate, C. C. Kiris, Validation of immersed boundary wall-modelled large eddy simulations with F-16XL flight data, AIAA Aviation Forum (2024). https://doi.org/10.2514/6.2024-4374